EFFECTS OF LEADING EDGE GEOMETRY ON THE FLOW AROUND ELONGATED BLUFF BODIES

Zachary J. Taylor and Gregory A. Kopp
Boundary Layer Wind Tunnel Laboratory
University of Western Ontario
London, Ontario, Canada, N6A 5B9
ztaylor@uwo.ca and gakopp@uwo.ca

Roi Gurka
Department of Chemical Engineering
Ben Gurion University
Beer-Sheva, Israel, 84105
gurka@bgu.ac.il

ABSTRACT

We perform three-dimensional pressure experiments on elongated bluff bodies at $Re=5x10^4$. The results show unexpected trends in the aerodynamic loading of these bodies. To explain these trends, we analyze the three-dimensionality of the flow at various locations on each body as well as details of the wake recirculation region. The importance of the balance between leading and trailing edge flows is emphasized by these results and evidence of synchronization between the flow at these two locations is presented.

INTRODUCTION

Bluff body aerodynamics is a classical topic which has been extensively studied (e.g., Zdravkovich, 1997). The emphasis over the course of these studies has been on the circular cylinder for its geometric simplicity and engineering importance.

There exist another class of bluff geometries, called elongated bluff bodies. The complexity of the flow around elongated bluff bodies is the result of the interaction between two significant classical shear flows. The first is vortex shedding wakes and the second is separating-reattaching flow at the leading edge. Thus, our definition of elongated bluff bodies is such that the flow must separate at the leading edge, followed by flow reattachment along the body and subsequent flow separation at the trailing edge. Not only do these bodies lead to design challenges of long-span suspension bridges (e.g., Ricciardelli, 2003), they also represent a fundamental flow which can increase our understanding of bluff body aerodynamics.

The study of Nakamura and Nakashima (1986) was among the first to show the uniqueness of these bodies. They installed a splitter plate in the wake and were able to observe what looked like a vortex street. This flow feature was linked to a shear layer instability in cavity flows and was later renamed the Impinging Leading Edge Vortex (ILEV) instability by Naudascher and Wang (1993). This instability has been studied almost exclusively for low Reynolds number rectangular cylinders. Nakamura et al. (1991) showed that the ILEV instability caused a stepwise change in the Strouhal number with increasing elongation (or chord-to-thickness, *c/t*) ratio if the Strouhal number is defined by the chord. In terms of explaining the mechanism of the ILEV instability, Hourigan et al. (2001) emphasized the importance of the trailing edge vortex shedding in controlling the ILEV instability. Later, Mills et al. (2003) performed perturbation experiments to understand the balance of leading and trailing edge vortex shedding. They found that if the leading edge shedding was forced at a frequency far from the natural (unperturbed) shedding frequency, the trailing edge shedding was suppressed. The findings of Mills et al. (2003) are in agreement with those of Parker and Welsh (1983).

Parker and Welsh (1983) found that for a wide range of elongation ratios, vortex shedding was suppressed altogether. These observations were for Reynolds numbers of $1.5\text{-}3x10^4$ where the ILEV instability is suppressed for rectangular cylinders (Nakamura et al., 1991). With the increasing amount of energy at more frequencies, as Reynolds numbers increase, the pressure pulse from the trailing edge is thought to be suppressed and for the elongation ratio range of $6 < c/t < 25$, the spectra of the wakes are markedly different (Parker and Welsh, 1983). However, there are examples of flows around elongated bluff bodies other than rectangular cylinders (e.g., Welsh et al., 1984; Nguyen and Naudascher, 1991) at similar Reynolds numbers, where vortex shedding is detected. Thus, the effect of geometry – and in particular leading edge geometry (Nguyen and Naudascher, 1991) – is a critical parameter in determining the existence and character of vortex shedding of elongated bluff bodies. However, the mechanisms controlled by the geometry are not well elucidated. Furthermore, the persistence of the ILEV instability for other geometries at higher Reynolds numbers remains an open question.

Taylor et al. (2011) examined three distinct geometries, all with elongation ratios of 7, at a Reynolds number of $3x10^4$. The results were framed in the context of the momentum balance of the recirculation region. Markedly different dynamics were found using this method. It was shown that

the Reynolds shear stresses were as important at closing the recirculation region as the base pressure for bodies with significant leading edge separation. In the classical literature on bluff body aerodynamics (e.g., Roshko, 1954), it is shown that the base pressure dominates the closure of the recirculation region. It is also the base pressure which is commonly used to show the strength of vortex shedding. However, Taylor et al. (2011) show that the dynamics of the recirculation region for elongated bluff bodies are more complex. Because of the separation at the leading edge, the boundary layers at the trailing edge are inherently turbulent and contain vorticity generated at the leading edge.

The importance of the Reynolds shear stresses at the boundary of the recirculation region highlights the importance of momentum transfers from the flow outside of the recirculation region (the "outer" flow) and that inside (the "inner" flow). This balance was examined further in Taylor et al. (submitted for publication) where proper orthogonal decomposition revealed the existence of a separated shear layer mode for these bodies. This mode was shown to reflect the balance of outer and inner flows and was directly related to the fluctuating flow distribution at the edge of the recirculation region.

An open question related to the balance of inner and outer flows at these higher Reynolds numbers regards the three-dimensionality of the flow. The ILEV instability is largely conceptualized as a two-dimensional flow phenomenon with the leading edge vortices interacting with those at the trailing edge (e.g., Mills et al., 2003). At lower Reynolds numbers, it is expected that the spanwise correlation is strong for these vortices. However, at higher Reynolds numbers it remains unclear if it is the increased three-dimensionality of the flow which destroys the ILEV instability or whether the synchronization between leading and trailing edge is suppressed. The objective of the current paper is to address this question.

EXPERIMENTAL SETUP

Surface pressures

Experiments were performed on 6 different geometries. All geometries had a constant thickness, t, (measured vertically) of 76.2 mm and a constant span of 1.83 m. The distance from leading edge separation to trailing edge separation was also held constant at 533.4 mm, or, 7t. It is this measure which will be referred to as the chord length, c, of the model rather than the distance from the tip of the nose to the trailing edge. To create the 6 distinct geometries, different noses were fitted to the leading edge with the blunt (square-edged) trailing edge held constant. Five of the noses were of triangular cross-section with varying interior angles. These noses created fixed separation points. An elliptical nose with a 3:1 ratio was also used to include a case with no leading edge separation. Details of these models are presented in Table 1.

The models were all tested in a large wind tunnel at the Boundary Layer Wind Tunnel Laboratory. The models were placed shortly after the contraction of a closed circuit wind tunnel with a cross-section of 1.83 m x 3.35 m and a length of 39 m. End plates were fitted to each model on either side extending approximately one chord into the wake. The velocity profiles measured at this location show turbulence intensity that is under 1% and the velocity profile is uniform to within 1%. The free stream speed was adjusted to yield Reynolds numbers between $4x10^4$ – $7.5x10^4$, based on the model thickness.

The pressure data were collected via 512 surface pressure taps on the body. The layout of these taps is shown in Figure 1. There are three streamwise loops around the body including one in the centre of the body. There are also 5 spanwise rows: two along each of the top and bottom as well as one row along the base of the model. The spanwise rows all have the same tap spacing as each other. Close to the centre of the model, the taps are spaced 15.9 mm apart while farther from the centre the spacing is 25.4 mm. The streamwise rings have a higher density of taps (spaced 15.9 mm apart) within the leading edge recirculation bubble.

Table 1. Details of the models used in the pressure experiments

Model	Interior Nose Angle	Separation Angle
1	(Ellipse)	0
2	60	30
3	90	45
4	120	60
5	150	75
6	180	90

The 512 taps were connected to multiplexed pressure scanners. The tubing system from the tap to the transducer is measured to have a frequency response which is flat to beyond 180 Hz by a random frequency generator. The data was interpolated over very short time steps which is necessary due to the multiplexed system. Phase lag measurements ensure that this process has a negligible effect on the data (Ho et al., 1999). The pressure data were collected at a sampling frequency of 500 Hz for 120 sec. and low pass filtered at 180 Hz.

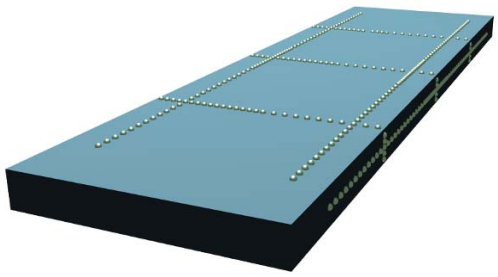

Figure 1. Schematc of the pressure tap layout of the model. Camera is looking at the trailing edge and top of the model.

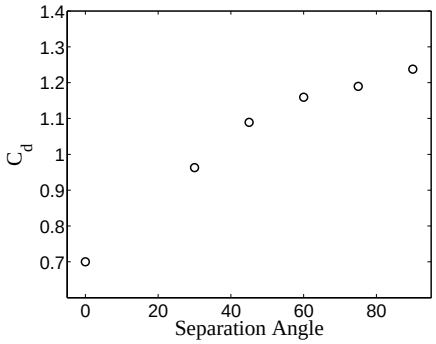

Figure 2. Variation of the sectional drag coefficient with separation angle

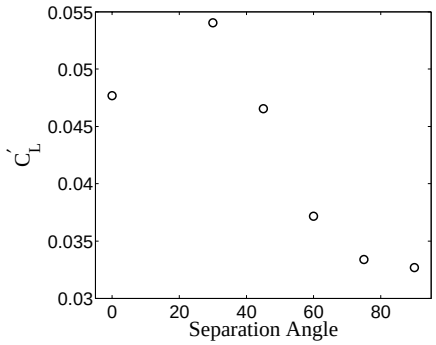

Figure 3. Variation of the sectional rms lift coefficient with separation angle.

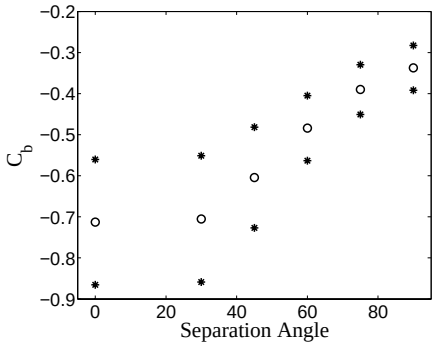

Figure 4. Variation of base pressure with separation angle. Open symbols are the mean and * mark the standard deviation from the mean.

Particle Image Velocimetry

The pressure data are supplemented by Particle Image Velocimetry (PIV) measurements made on three similar elongated bluff bodies. These bodies all share the elongation ratio of the body used in the pressure measurements; however, the leading and trailing edges of the three models are symmetric and are of square, triangular and semi-circular cross-sections (for details refer to Taylor et al., 2011).

The data are measured at a Reynolds number of $3x10^4$ in open-return wind tunnel with dimensions 0.46 x 0.46 m^2. The flow was seeded with atomized olive oil. The PIV system is comprised of a Nd:YAG laser with a pulse energy of 120 mJ and wavelength of 532 nm. The cameras are of CCD type with a 12-bit dynamic range. The sampling frequency of the PIV system is slow and shown to be sporadic so the 5000 image pairs captured are treated as statistically independent samples.

RESULTS

For the pressure measurements shown, we include only one ($Re=5x10^4$) of the eight Reynolds numbers at which measurements were made.

Aerodynamic loads

The sectional lift and drag forces are obtained by integration of the pressure taps along the surface of the body. Since each pressure tap is sampled nearly simultaneously (see "Surface pressures" section for details), it is possible to obtain an estimate of the sectional lift and drag forces at each sample in time. The mean sectional drag coefficient is plotted versus separation angle in Figure 2. The drag force is observed to increase monotonically with separation angle, as would be expected, due to the increased bluffness of the leading edge. Due to the symmetry of the models tested, the mean lift force is negligible; however, the lift fluctuations are not, as shown in Figure 3. There is an observed peak in the strength of the lift fluctuations for a separation angle of 30° followed by a steady decrease as separation angle increases. This trend in the lift fluctuations is an important point which is addressed in the Discussion.

While only the data of the centre ring are shown herein, the data of the other streamwise rings of pressure taps confirm the presented results. The three-dimensionality of the data is discussed in the section "Spanwise characteristics" below; however, in the time-averaged sense the data is well correlated along the span.

Base pressure and shedding frequency

The base pressure is measured at the mid-height of the trailing edge surface. It has traditionally been used as an estimate to gauge the strength of the vortex shedding (Roshko, 1954). The base pressure is plotted here in Figure 4. In Figure 4 we have marked the standard deviation of the base pressure plotted offset from the mean. It is observed that models 1 & 2 (see Table 1 for the definition of these labels) have similar base pressure measurements while the suction and corresponding fluctuations decrease as leading edge separation angle is increased.

Shedding frequency is normalized by the Strouhal number using the thickness of each model, $St=ft/U_\infty$. To show the dependence of the main feature of the flow – the vortex shedding – on the Reynolds number, the frequency measured at all 8 Reynolds numbers is plotted against the separation angle in Figure 5. The trend in the Strouhal number is nearly linearly decreasing with leading edge separation angle.

Spanwise characteristics

The surface pressure measurements extended towards the whole span of the model thus ensuring a reliable

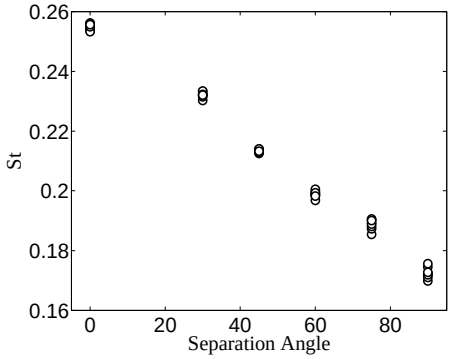

Figure 5. Strouhal number variation with separation angle at all tested Reynolds numbers.

representation of the three-dimensionality of the flow around the body.

To demonstrate how well the flow is correlated along the body we calculated the spatial correlation of the pressure,

$$R(\zeta) = \frac{\overline{p'(z_0,t)p'(z_0+\zeta,t)}}{\sigma_p^{\,2}} \qquad (1)$$

at different locations in Figure 6, for each model. In Eq. 1, z_0 represents the spanwise centre of the model and ζ is the spatial lag. The prime denotes a pressure fluctuation in time and the overbar represents a time-average. Only half of the span is shown in Figure 6 due to the symmetry of the result.

The data shown in Figure 6 (a)-(c) are for the spanwise rows at the leading edge, trailing edge and base, respectively. Near the leading edge (x/t=1 from the separation point), the models with larger separation angles are shown to have higher correlation along the span. The situation is reversed near the trailing edge (x/t=6) where models with small separation angles have high spanwise correlation. Along the base of the model (y/t=0), all models have approximately the same spanwise correlation with the correlation dropping off quickly from $R(\zeta)$=1 with spanwise distance.

Recirculation region

We define the recirculation region herein, as the region in the near wake contained within the separating streamlines at the trailing edge. These streamlines extend from the trailing edge of the body and join at a saddle point in the wake which marks the end of the recirculation region (Taylor et al., 2011).

It is the recirculation region where the interaction occurs between the trailing edge boundary layer and the development of trailing edge vortices. As mentioned previously, the base pressure is classically used as a measure of the strength of vortex shedding. The base pressure has been reported in Figure 4. However, the distribution of base pressure along the trailing edge is also available from the present dataset. The mean pressure distribution is nearly flat along the trailing edge surface; yet, the *rms* of the pressure coefficients, C_p', is not and is shown in Figure 7. It is observed that even though models 1 & 2 share a similar base pressure (and similar C_p' at the base location) that further away from the centre of the trailing edge, there are noticeable differences. Also distinct is the rate at which the C_p' increases away from the centre at the trailing edge for model 2.

To explore the flow mechanisms for the observed differences in the distribution of pressure at the recirculation region, we use the results of the PIV experiments. An ensemble average is performed by identifying image pairs where there is a vortex present in a small window. The window is located at one third of the length of the recirculation region for all 3 models. It is defined narrowly in the x-direction as 0.25t with a more relaxed dimension in the y-direction (0.5t). Vortices are identified by their "swirling strength" (Adrian et al., 2000) which is the complex portion of the eigenvalue of the 2D velocity gradient tensor. A suitable threshold is applied to include an identified vortex in the ensemble average. The result of this ensemble average is shown in the form of vorticity contours with streamlines superimposed in Figure 8.

From Figure 8, it is observed that a large trailing edge vortex is formed for the model with circular leading and trailing edges. It is also shown to travel further down into the recirculation region than for the other two models (Taylor et al., 2011). The model with square leading and trailing edges is observed to have a small vortex formed near the top of the recirculation region and the model with triangular leading and trailing edges is between these two cases.

Synchronization

The disappearance of the ILEV instability at Reynolds numbers above 2000 is well documented for rectangular cylinders of similar elongation ratio (e.g., Nakamura et al.,

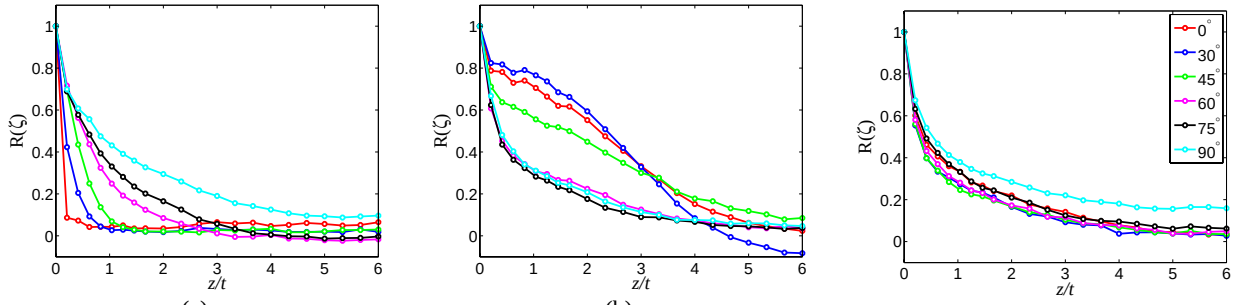

Figure 6. Spanwise correlation at: (a) leading edge, (b) trailing edge, (c) base of the model. The separation angles are marked with differing colours (refer to legend in (c) for all 3 plots).

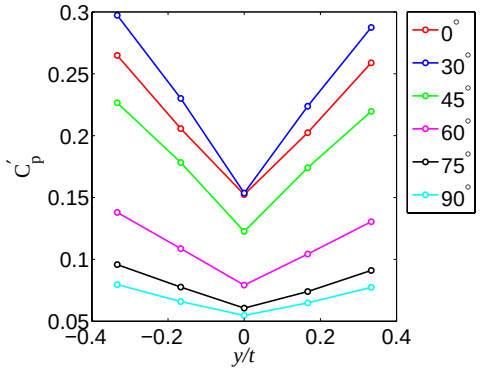

Figure 7. Fluctuating base pressure along the trailing edge of each model.

1991; Parker and Welsh, 1983). However, there is a lack of information on its persistence for other geometries.

To investigate the possible synchronization between the shedding from the leading edge and the shedding from the trailing edge, a cross-correlation with a temporal lag has been performed. This cross-correlation is performed between a tap within the separation bubble on the top of the model at the leading edge (location 1) and a pressure tap near the top of the recirculation region (location 2) as follows,

$$R(\tau)=\frac{\overline{p'(\bar{x}_1,t)p'(\bar{x}_2,t+\tau)}}{\sigma_{x_1}\sigma_{x_2}} \qquad (2)$$

The result of this cross-correlation is shown in Figure 9. The time lag on the x-axis is normalized by each model's shedding period, T_s. It is evident that while model 6 has the highest correlation coefficient, the two locations show little synchronization. Models 2-5 (model 1 has no leading edge separation and is not included in the figure), meanwhile, show good synchronization between the two pressure taps. It is also observed that the weakest synchronization among models 2-5 is model 5 which could indicate it is beginning to transition to a state similar to model 6.

DISCUSSION

The study performed herein is a systematic examination of the effect of leading edge separation angle on elongated bluff bodies. The change in the drag coefficient was anticipated to increase with increasing separation angle as has been observed. The fluctuating lift coefficient, however, shows that there exists a separation angle (30°) where the fluctuating lift coefficient is maximum. It was observed to peak without a similar peak in the shedding frequency or base pressure. For shorter bluff bodies, the base pressure, shedding frequency and lift fluctuations all tend to vary with each other because they represent the strength of vortex shedding (Roshko, 1954). However, it is shown herein that these trends do not apply to elongated bluff bodies.

It is suggested that the main reason that the trends from shorter bluff bodies do not translate for elongated bluff bodies is the balance between the leading edge shedding and that occurring at the trailing edge. Taylor et al. (2011) showed that the balancing dynamics of the recirculation region are indeed distinct for elongated bluff bodies. It was shown that the importance of the pressure field diminishes in balance with the turbulent momentum transfers at the edge of the recirculation region. The interaction occurring at the edge of the recirculation region is suggested to be coupled between the leading and trailing edge vortices. If the leading edge vortex is large it is expected to dominate and "absorb" the growing trailing edge vortex. Assuming this mechanism occurs, one would expect a preference for trailing edge vortex position higher in the recirculation region, i.e., closer to the "outer" flow. The ensemble average shown in Figure 8 suggests that this mechanism is occurring. The results in Figure 7 show that even though the base pressure is approximately the same between models 1 and 2, that model 2 has a noticeably higher fluctuating pressure away from the centre of the trailing edge which would also be indicative of a vortex being closer to the outer flow. The high C_p, combined with the strength of the lift fluctuations, show that model 2 sheds the strongest vortices. Thus, the interaction with the flow from the leading edge is observed to enhance shedding for this model.

The importance of the synchronization of the leading and trailing edge flows on their balance was highlighted by Mills et al. (2003). We have shown that the leading edge separation bubble is not synchronized with the trailing edge vortex shedding (Figure 9) for model 6; however, it would appear that the synchronization exists for all other geometries. This synchronization suggests the persistence of the ILEV instability at higher Reynolds numbers. Nakamura et al. (1991), among others, have implied that it was the Reynolds number which caused the suppression of the ILEV instability. However, the present results suggest that geometry could have a greater effect on the persistence of the ILEV instability. The subtle difference in separation angle between models 5 and 6 is observed to be enough to suppress the instability. The dynamics of the flow between these two cases which cause this suppression are of interest. A potential explanation for the

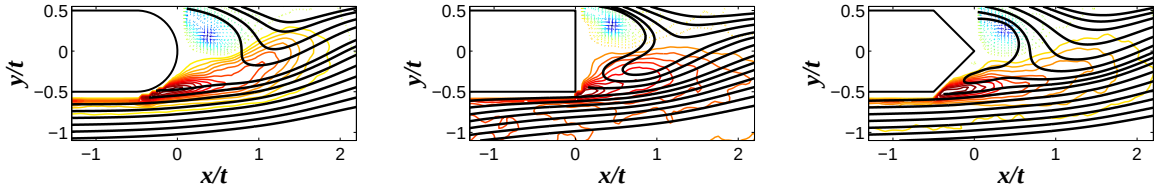

Figure 8. Ensemble average (based on vortex position) of the recirculation region of the three symmetric elongated bluff bodies.

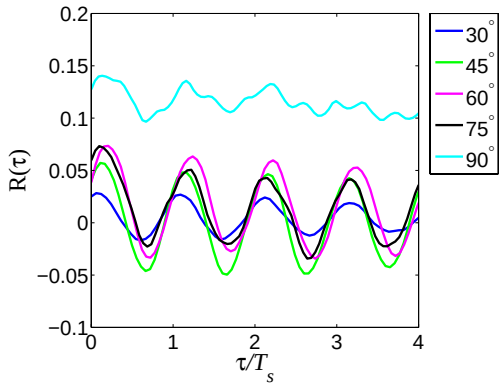

Figure 9. Cross-correlation between leading edge and trailing edge separation regions.

suppression of the ILEV instability has been the increased three-dimensionality of the flow at higher Reynolds numbers. However, the data presented herein show no marked change between model 5 and 6 in the correlation along the span of the model. The spanwise correlation along the base of the model was actually shown to be the same for all 6 models tested herein. Due to the observation that all models shared the poor correlation in the base region it is difficult to conclude that large scale three-dimensional effects are governing the instability. The effect of increased small scale activity at these higher Reynolds number is a subject for future investigation.

CONCLUSION

We have shown that elongated bluff bodies do not share trends established for shorter bluff bodies. The spanwise correlations showed that the flow was well correlated at the leading edge for bodies with large separation angles and better correlated at the trailing edge for bodies with smaller separation angles. For all cases, the flow within the recirculation region was shown to be poorly correlated. The spanwise data reveals that it is unlikely that large scale three-dimensional effects are responsible for the disappearance of the ILEV instability for rectangular cylinders at this Reynolds number.

The recirculation region emphasized the distinctions among many of the models. It was shown that model 2 had the strongest fluctuating base pressure and also had strong vortices forming farther away from the centreline than model 1. An ensemble average based on vortex position of similar models illustrated this flow mechanism.

It was shown herein that for Reynolds numbers $O(10^4)$, that only the model with a separation angle of 90° did not have synchronized shedding between the leading and trailing edges. This result is consistent with the literature which suggests that the ILEV instability is undetectable for rectangular cylinders past a Reynolds number of 2000. However, the present results suggest that geometry also has a significant effect on the synchronization between leading and trailing edge shedding.

REFERENCES

Adrian, R., Christensen, K. and Liu, Z., 2000, "Analysis and interpretation of instantaneous turbulent velocity fields", *Experiments in Fluids*, Vol. 29, pp. 275-290.

Ho, T.C.E., Lythe, G.R., Isyumov., N., 1999, "Structural loads and responses from the integration of simultaneous pressures". In: *Proceedings of the 10th International Conference on Wind Engineering*. Copenhagen, Denmark, pp. 1505-1510.

Hourigan, K., Thompson, M. C. and Tan, B. T., 2001, "Self-sustained oscillations in flows around long blunt plates", *Journal of Fluids and Structures,* Vol. 15, pp. 387-398.

Mills, R., Sheridan, J. and Hourigan, K., 2003, "Particle image velocimetry and visualization of natural and forced flow around rectangular cylinders", *Journal of Fluid Mechanics,* vol. 478, pp. 299-323.

Nakamura, Y., Ohya, Y. and Tsuruta, H., 1991, "Experiments on vortex shedding from flat plates with square leading and trailing edges", *Journal of Fluid Mechanics* Vol. 222, pp. 437-447.

Nakamura, Y. and Nakashima, M., 1986, "Vortex excitation of prisms with elongated rectangular, H and T cross-sections", *Journal of Fluid Mechanics,* Vol. 163, pp. 149-169.

Naudascher, E. and Wang, Y., 1993, "Flow-induced vibrations of prismatic bodies and grids of prisms", *Journal of Fluids and Structures,* Vol. 7, pp. 341-373.

Nguyen, T. D. and Naudascher, E., 1991, "Vibration of beams and trashracks in parallel and inclined flows", *Journal of Hydraulic Engineering*, Vol. 117, pp. 1056-1076.

Parker, R. and Welsh, M., 1983, "Effects of sound on flow separation from blunt plates", *International Journal of Heat and Fluid Flow*, Vol. 4, pp. 113-127.

Ricciardelli, F., 2003, "On the wind loading mechanism of long-span bridge deck box sections", *Journal of Wind Engineering and Industrial Aerodynamics*, Vol. 91, pp. 1411-1430.

Roshko, A., 1954, "A new hodograph for free-streamline theory", *NACA Technical Note 3168*, National Advisory Committee for Aeronautics.

Taylor, Z.J., Palombi, E., Gurka, R. and Kopp, G.A., 2011, "Features of the turbulent flow around symmetric elongated bluff bodies", *Journal of Fluids and Structures* Vol. 27, pp. 250-265.

Taylor, Z.J., Gurka, R. and Kopp, G.A., Submitted for publication, "Wake structure of elongated bluff bodies using proper orthogonal decomposition", *Submitted: Physics of Fluids*.

Welsh, M., Stokes, A. and Parker, R., 1984, "Flow-resonant sound interaction in a duct containing a plate, part 1: Semi-circular leading edge", *Journal of Sound and Vibration*, Vol. 95, pp. 305-323.

Zdravkovich, M.M., 1997, Flow around circular cylinders: Volume 1, Oxford University Press.